CHEMISTRY OF MATERIALS
Cite This: Chem. Mater. 2018, 30, 7047−7054
Article
pubs.acs.org/cm

Dynamic Ferrimagnetic Order in a Highly Distorted Double Perovskite Y_2CoRuO_6

Zheng Deng,[†,‡] Maria Retuerto,[§] Sizhan Liu,[∥] Mark Croft,[⊥] Peter W. Stephens,[#] Stuart Calder,[▽] Wenmin Li,[‡] Bijuan Chen,[‡] Changqing Jin,[‡] Zhiwei Hu,[○] Man-Rong Li,[†,◆] Hong-Ji Lin,[¶] Ting-Shan Chan,[¶] Chien-Te Chen,[¶] Sun Woo Kim,[†,△] and Martha Greenblatt*[,†]

[†]Department of Chemistry and Chemical Biology, Rutgers, The State University of New Jersey, 610 Taylor Road, Piscataway, New Jersey 08854, United States
[‡]Institute of Physics, School of Physics, University of Chinese Academy of Sciences, Chinese Academy of Sciences, P.O. Box 603, Beijing 100190, China
[§]Grupo de Energía y Química Sostenibles, Instituto de Catálisis y Petroleoquímica, CSIC, C/Marie Curie 2, L10, 28049, Madrid, Spain
[∥]Department of Physics, New Jersey Institute of Technology, Newark, New Jersey 07102, United States
[⊥]Department of Physics and Astronomy, Rutgers, The State University of New Jersey, 136 Frelinghuysen Road, Piscataway, New Jersey 08854, United States
[#]Department of Physics & Astronomy, State University of New York, Stony Brook, New York 11794, United States
[▽]Neutron Scattering Division, Oak Ridge National Laboratory, Oak Ridge, Tennessee 37831, United States
[○]Max-Planck Institute for Chemical Physics of Solids, Nöthnitzer Straße 40, 01187 Dresden, Germany
[◆]Key Laboratory of Bioinorganic and Synthetic Chemistry of Ministry of Education, School of Chemistry, Sun Yat-Sen University, Guangzhou 510275, China
[¶]National Synchrotron Radiation Research Center, Hsinchu 30076, Taiwan, R.O.C.
[△]Department of Chemistry Education, Chosun University, Gwangju 61452, South Korea

Supporting Information

ABSTRACT: Y_2CoRuO_6 was synthesized as a *B*-site ordered double perovskite with distorted monoclinic $P2_1/n$ symmetry and an average tilting of the CoO_6 and RuO_6 octahedra of $\bar{\psi}$ = 19.7°. DC magnetization measurements show a ferrimagnetic transition at around 82 K. Although long-range ferrimagntic order is supported by neutron diffraction studies, aging phenomena in time-dependent isothermal magnetization, frequency dependence of AC susceptibility, and a smeared peak in the specific heat together reveal spin glass-like dynamics. The magnetic subtleties resemble chaotic behavior as previously observed in some ferro- or ferrimagnetic materials that exhibit spin glass-like dynamics. It is argued that the magnetic dynamics in Y_2CoRuO_6 mainly stem from competition between antiferromagnetic Co↑-O-(Ru)-O-Co↓/Ru↑-O-(Co)-O-Ru↓ and antiferromagnetic Co↑-O-Ru↓ interactions, besides a degree of Co:Ru antisite disorder. Herein, the *B*-site ordered Y_2CoRuO_6 offers a model to explore the intriguing dynamics in correlated 3*d*−4*d* transition metal double perovskites.

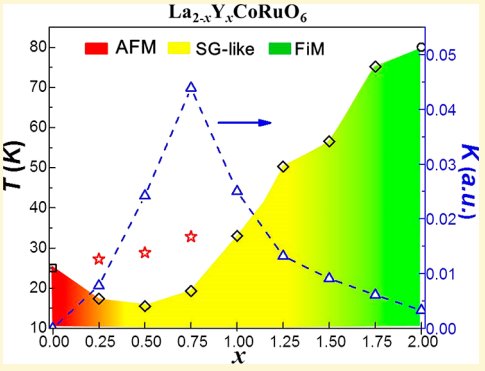

INTRODUCTION

Magnetically frustrated materials have been investigated extensively due to their exotic magnetic states such as spin liquid, spin ice, and spin glass (SG).[1−3] Interestingly, intrinsic dynamics of long-range magnetic order (e.g., ferromagnetic, FM) have been found in a few magnetic materials (e.g., $(Fe_{0.20}Ni_{0.80})_{75}P_{16}B_6Al_3$) where magnetic frustration is inherent.[4,5] These so-called "chaotic" magnetic systems exhibit dynamic features similar to the SG phase. When the frustration is weak, the long-range magnetic order still persists. On increasing frustration above some threshold value, the long-range magnetic order is either no longer energetically favorable or kinetically accessible. In such case, the low temperature phase is the spin glass phase, with transition to a long-range magnetic ordered state at higher temperature.

Received: June 27, 2018
Revised: September 24, 2018
Published: September 24, 2018

DOI: 10.1021/acs.chemmater.8b02728
Chem. Mater. 2018, 30, 7047−7054

The *B*-site ordered $A_2BB'O_6$ double perovskites, with rich magnetic properties, due to the variety of possible combinations of *B*- and *B*′-site transition metal cations, are outstanding models to study magnetic dynamics and frustration. In *B*-site ordered double perovskites, when magnetic cations only reside on the *B*′-site, and form a face-centered cubic sublattice, typically, geometrical frustration is observed. Contrasting unique magnetic ground states have been observed experimentally, including an antiferromagnetic (AFM) state in Ba_2YRuO_6 and Ba_2YOsO_6,[6,7] spin freezing without long-range order in Ba_2YReO_6 and Sr_2MgReO_6,[8,9] a collective singlet state coexisting with paramagnetism in Ba_2YMoO_6 and an FM Mott-insulating state in Ba_2NaOsO_6.[10,11] AFM and FM orders were found in Sr_2CrSbO_6 and Ca_2CrSbO_6, respectively.[12]

In the case of two magnetic *B*-sites, interactions between them become more complicated. The Goodenough−Kanamori (GK) rules can predict magnetic properties of insulating double perovskites where *B* and *B*′ are 3*d* transition metals, but they are unreliable for systems with *B* = 3*d* and *B*′ = 4*d*/5*d*.[13] Therefore, studies of new magnetic 3*d*−4*d* double perovskites are intriguing and topical. Recently, two types of AFM superexchange, *B*↑-O-*B*′↓ and *B*↑-O-(*B*′)-O-*B*↓/*B*′↑-O-(*B*)-O-*B*′↓, were reported in $(Sr,Ca)_2MOsO_6$ compounds with *M* = Cr, Fe, and Co.[14−16] In the ideal cubic double perovskite structure, both the *B*- and *B*′-sites form face-centered cubic lattices. In practice, double perovskites usually exhibit structural distortions from the cubic symmetry most commonly caused by introducing a small cation into the *A*-site. Accordingly, the lattice compression often lowers the crystal symmetry from cubic to tetragonal or monoclinic, and simultaneously tilts the BO_6 and $B'O_6$ octahedra (namely, bends *B*-O-*B*′ angle). The *B*↑-O-*B*′↓ AFM superexchange is known to be highly sensitive to bond angle. In $(Sr,Ca)_2CoOsO_6$, the bent Co−O−Os angles favor the Co↑-O-Os↓ pathway and enhance the ground state changes from AFM in Sr_2CoOsO_6 to SG in $SrCaCoOsO_6$ and finally to ferrimagnetism (FiM) in Ca_2CoOsO_6.[15]

Although diverse magnetic states are known to be produced by lattice compression in $A_2BB'O_6$, the details of the magnetic properties of each magnetic phase are not known. In this article, we report a new double perovskite compound Y_2CoRuO_6 with combination 3*d* and 4*d* metals at *B*-sites. In Y_2CoRuO_6, highly bent Co−O−Ru angles ($\overline{\phi}$ = 141.7°) give rise to robust Co↑-O-Ru↓ AFM interactions with a FiM Curie temperature (T_C) close to 82 K. Regardless of a long-range FiM order determined by neutron powder diffractions (NPD), the DC and AC magnetizations reveal intrinsic dynamics of the FiM order. Further studies on selected solid solutions of ($La_{2-x}Y_xCoRuO_6$, $0 \le x \le 2$) imply that competition between the two aforementioned superexchange interactions mainly contributes to the dynamic features in Y_2CoRuO_6.

EXPERIMENTAL SECTION

Synthesis. Polycrystalline samples were synthesized by conventional solid state reaction with high purity starting materials. The well-ground mixture of Y_2O_3 (Alfa Aesar, 99.9%), La_2O_3 (Alfa Aesar, 99.9%, calcined at 1300 K before usage), Co_3O_4 (Alfa Aesar, 99.7%), and RuO_2 (Alfa Aesar, 99.9%) was pelletized and then calcined between 1400 and 1500 K for 24 h. After intermediate grinding, the recovered pellets were pressed into pellets again and calcined for another 24 h at 1500 K. It is worth noting that all the samples are homogeneous according to chemical composition analysis by EDX (Figures S1−S3 and Tables S1−S3).

Laboratory Powder X-ray Diffraction (PXD), Synchrotron Powder X-ray Diffraction (SPXD), and Neutron Powder Diffraction (NPD). Phase purity of all the samples was established with laboratory PXD. The high scattering contrast of Co and Ru to X-ray allows us to analyze the antisite ratio of *B*- and *B*′-sites. SPXD of Y_2CoRuO_6 was conducted at beamline 11-BM of APS at Argonne National Laboratory. NPD measurements at 10, 80, and 150 K were carried out at the beamline-HB-2A, Oak Ridge National Laboratory (ORNL). Rietveld refinements were performed using the GSAS and FullProf software packages.[17−19]

X-ray Absorption Near-Edge Spectroscopy (XANES). The $L_{2,3}$-edge measurements on Y_2CoRuO_6 compound (and selected standards) were performed at the National Synchrotron Radiation Research Center in Taiwan at the Taiwan Light Source (TLS): the Co $L_{2,3}$-edges at beamline 11A with a spherical grating monochromator, and the Ru $L_{2,3}$-edges at beamline 16A with a double crystal Si(111) monochromator. The Co *K*-edge measurements on the Y_2CoRuO_6 were performed (with a simultaneous standard) at NSLS-II on the Inner Shell Spectroscopy (ISS) insertion device (damping wiggler) 8-ID beamline with a Si(111) double crystal high-heat load monochromator operated in an extremely rapid continuous energy variation mode. The multiple Ru $L_{2,3}$ standard and Co *K* standard spectra were collected at NSLS-I on beamline X19A with a Si(111) double crystal monochromator. The spectra were fit to linear pre- and postedge backgrounds and normalized to unity absorption edge-step across the edge with the exception of the Co $L_{2,3}$-edges which were normalized to the highest peak in the absorption spectra. Most of the spectra were collected in the fluorescence mode. Some of the spectra were collected in the total electron yield mode.

DC Magnetization. DC magnetization measurements were conducted with a Quantum Design Superconducting Quantum Interference Device-Vibrating Sample Magnetometer (SQUID-VSM). Temperature-dependent magnetization ($M(T)$) was measured under zero field cooled (ZFC) and field cooled (FC) procedures. Magnetic field dependence of magnetization ($M(H)$) was collected in a field range of ±7 T at selected temperatures. Time-dependent isothermal magnetization $M(t)$ was performed as ZFC relaxation in which the sample was cooled to measuring temperature in the ZFC procedure from room temperature. The sample was kept under zero field for different waiting times (t_w) at measuring temperature. Then, $M(t)$ data were collected with a small field (10 Oe).

AC Susceptibility, Heat Capacity, and Resistivity. AC susceptibility, resistivity, and heat capacity measurements were conducted with a Quantum Design Physical Property Measurement System (PPMS). AC susceptibility was measured under a zero DC background field with an amplitude of 6 Oe for different frequencies. Heat capacity measurements were collected on a sintered pellet mounted with Apiezon grease. Resistance measurements were performed with a standard four-probe technique.

Energy Dispersive X-ray Spectroscopy (EDX). Chemical composition analysis was performed on a commercial scanning electron microscope (SEM) with energy dispersive X-ray spectroscopy.

RESULTS

Y_2CoRuO_6. *Crystal Structure.* The crystal structure of Y_2CoRuO_6 was determined from SPXD data at room temperature and from NPD data at 150, 80, and 10 K. All of the diffraction patterns contain a small amount of Y_2O_3 (~1% in weight) according to the Rietveld refinement as shown in Figure 1a and Figure S5. Y_2CoRuO_6 is isostructural to La_2CoRuO_6 with monoclinic $P2_1/n$ symmetry as shown in Figure 1b. The Co and Ru cations alternately occupy the octahedral sites with $a^-a^-b^+$ tilting, as defined by Glazer notation.[20,21] Refinement parameters and structural details are listed in Table 1 and Table S4. Partial Co:Ru antisite ratios from both SPXD and NPD analyses are 16% and 8%, respectively, in Table 1. Since SPXD and NPD were performed

DOI: 10.1021/acs.chemmater.8b02728
Chem. Mater. 2018, 30, 7047−7054

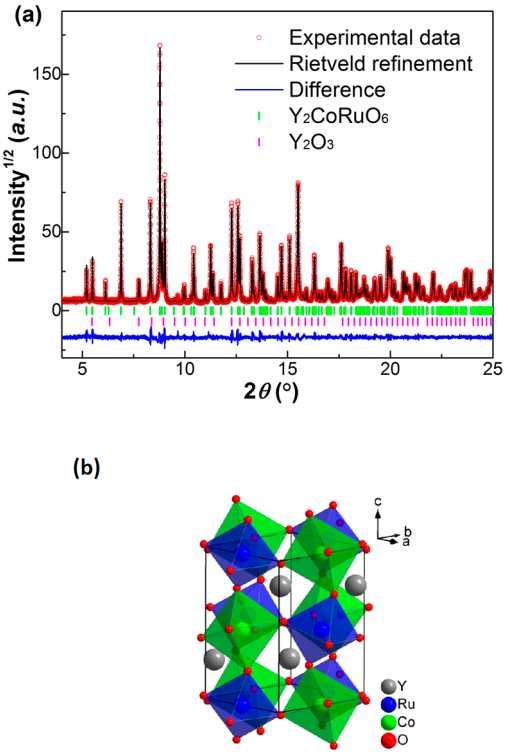

Figure 1. (a) Rietveld refined SPXD profiles of Y_2CoRuO_6 at room temperature. (b) The crystal structure of Y_2CoRuO_6.

on different samples, we believe that the different Co:Ru antisite ratios in Y_2CoRuO_6 are due to batch-to-batch variations and depend on synthesis conditions to some degree. The volume decreases with decreasing temperature as expected due to thermal contraction. The average octahedral tilt angle is defined as $\bar{\psi} \equiv (180 - \bar{\phi})/2 = 19.7°$, where ϕ is the interoctahedral Co−O−Ru angle. It shows an increased structural distortion compared with that of La_2CoRuO_6 ($\bar{\psi}$ = 13.4°).[22] The average bond lengths of Co−O (2.053(4) Å) and Ru−O (2.021(4) Å) are comparable to those of La_2CoRuO_6 (2.068(8) Å for Co−O and 1.998(8) Å for Ru−O).[22] Bond valence sum (BVS) is 2.21 for Co and 3.64 for Ru, which indicate the formal oxidation state of *B*-site cations as Co^{2+} (d^7) and Ru^{4+} (d^4).[23] The cation oxidation states have been corroborated by the X-ray absorption near edge spectroscopy (XANES) studies (Figure S4a−g)

Static Magnetism and Magnetic Structure. It should be noted that only minor and negligible divergences of physical properties have been found among Y_2CoRuO_6 samples with different Co:Ru antisite ratios. Thus, we only present results of the NPD sample (8% Co:Ru antisite) in the sections below, for the sake of simplicity. In Figure 2a, the sharp upturn of $M(T)$ at about 82 K indicates an FM-like phase transition. Below T_C, the divergence between ZFC and FC, which is suppressed by enhanced H, indicates the presence of magnetic frustration. In Figure 2b, the $M(H)$ curves also show FM-like characteristics with huge coercive fields (max $H_c \sim 2.5$ T) and large remnant moments (max $M_R \sim 0.73$ μ_B/f.u., which is close to the net moment of the antiparallel high-spin Co^{2+} (3 μ_B) and low-spin Ru^{4+} (2 μ_B)). All of these values shrink when the sample is warmed up.

Figure 2a also shows a hyperbola-like $\chi^{-1}(T)$ curve that is a feature of ferrimagnetism.[24] The Curie−Weiss law of eq 1 used for fitting the data in a high-temperature region (300−400 K)

$$\frac{1}{\chi} = \frac{T - \theta}{C} \tag{1}$$

where C is the Curie constant and θ is the paramagnetic temperature, yields C = 4.04 emu·K/mol/Oe, giving the paramagnetic effective moment μ_{eff} = 5.68 μ_B/f.u. and θ = −162 K. The μ_{eff} is comparable to that of La_2CoRuO_6.[25] The negative θ suggests dominant AFM interactions between Co^{2+} and Ru^{4+}. To further clarify the magnetic order in Y_2CoRuO_6, NPD data were collected and analyzed.

The magnetic structure was determined from the NPD data at 10 K, where magnetic diffraction peaks are clearly observed. All of the magnetic peaks appear at the positions of crystallographic Bragg reflections in space group $P2_1/n$,

Table 1. Select Structural Parameters As Determined from Rietveld Refinements

parameters	Y_2CoRuO_6-300 K#[a]	Y_2CoRuO_6-150 K*[a]	Y_2CoRuO_6-10 K*[a]
a/Å	5.2658(1)	5.2576(3)	5.2545(2)
b/Å	5.7107(1)	5.7121(3)	5.7112(3)
c/Å	7.5583(1)	7.5376(4)	7.5306(4)
β (deg)	90.033(1)	90.099(1)	90.036(1)
wt % of Y_2O_3	1.2	N/A	N/A
R_{wp} (%)	10.07	7.17	6.34
Co-Ru antisite	16.4(4)%	8(1)%	8(1)%
Co−O1 (×2) (Å)	2.066(4)	2.080(9)	2.068(8)
Co−O2 (×2) (Å)	2.045(4)	2.068(9)	2.075(9)
Co−O3 (×2) (Å)	2.050(4)	2.040(11)	2.020(11)
BVS-Co	2.21	N/A	N/A
Ru−O1 (×2) (Å)	2.039(4)	2.014(9)	2.017(8)
Ru−O2 (×2) (Å)	2.052(4)	2.036(9)	2.023(9)
Ru−O3 (×2) (Å)	1.972(4)	1.967(11)	1.987(11)
BVS-Ru	3.64	N/A	N/A
∠Co−O1−Ru (deg)	142.2(2)	142.9(3)	143.5(3)
∠Co−O2−Ru (deg)	143.0(2)	142.1(4)	142.5(4)
∠Co−O3−Ru (deg)	139.9(2)	140.3(4)	140.0(5)

[a]The ∗ represents data from NPD, and # represents data from SPXD.

DOI: 10.1021/acs.chemmater.8b02728
Chem. Mater. 2018, 30, 7047−7054

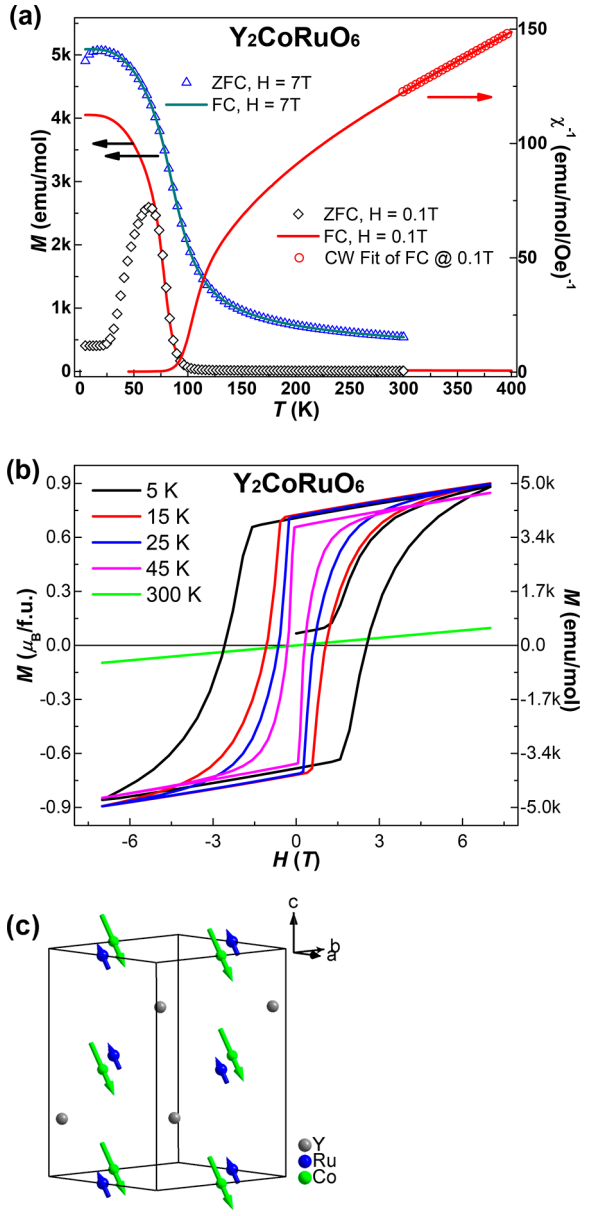

Figure 2. (a) Left *y*-axis corresponds to temperature dependence of DC magnetization with H = 0.1 and 7 T and the right one to inverse susceptibility with H = 0.1 T. (b) Field dependence of DC magnetization measured at various temperatures. (c) The magnetic structure of Y_2CoRuO_6 at 10 K. The spin directions are [1 0 −1] for Co spins (green) and [−1 0 1] for Ru (blue) spins.

corresponding to magnetic satellites defined by the propagation vector k = (0, 0, 0).

The two magnetic Co atoms of the unit cell are located at Co_1 ($^1/_2$, 0, $^1/_2$) and Co_2 (0, $^1/_2$, 0). The refinement shows that they are magnetically coupled in the following array: $m_{1x} = m_{2x} = 1.71(5)\ \mu_B$, $m_{1y} = m_{2y} = 0$, and $m_{1z} = m_{2z} = -1.71(5)\ \mu_B$. Similarly, the magnetic moments of the Ru atoms are located at Ru_1 ($^1/_2$, 0, 0) and Ru_2 (0, $^1/_2$, $^1/_2$), coupled as $m_{1x} = m_{2x} = -0.51(1)\ \mu_B$, $m_{1y} = m_{2y} = 0$, and $m_{1z} = m_{2z} = 0.51(1)\ \mu_B$, and oriented in the opposite direction from those of the Co spins. The global magnetic moments at 10 K have been refined as 2.42(6) μ_B at the Co positions and 0.71(2) μ_B at the Ru sites. Therefore, the magnetic structure can be described as two antiparallel ferromagnetic sublattices of Co and Ru spins stacked along [1 0 1] planes. Both antiparallel sublattices are arranged in a global long-range ferrimagnetic structure of Co and Ru magnetic moments. This magnetic arrangement leads to good agreement between observed and calculated magnetic intensities (Figure S5). Table 1 and Table S4 summarize the refinement parameters, and the magnetic structure is shown in Figure 2c. At 80 K, some magnetic reflections still emerge at about 30.5° and 32.3°, which indicate the existence of a significant degree of magnetic ordering.

Dynamic Magnetism. To elucidate the magnetic dynamics, AC susceptibility was measured with various applied frequencies (f). There is only one peak observed in real (M') and imaginary (M'') parts for each f at about 82 K in the temperature range of 2−110 K, consistent with the observed $T_C \sim 82$ K from DC $M(T)$. A selected temperature region (70−95 K) of the $M'(T)$ and $M''(T)$ is plotted in Figure 3a. The peaks in both $M'(T)$ and $M''(T)$ slightly move toward higher temperature with increasing f, for example, by 0.70 K from 113 to 9613 Hz in $M'(T)$. The frequency dispersion is a hallmark of SG-like dynamics. The frequency shift, K, is calculated to reflect the frequency dependence with eq 2[3]

$$K \equiv \Delta T_f / [T_f \Delta \log(f)] \quad (2)$$

where T_f is the magnetic ordering temperature at each f. The obtained value of $K \sim 0.0045$. However, for a canonical SG system, K ranges between 0.005 and 0.08.[26] The relatively smaller K obtained here suggests that the magnetic order in Y_2CoRuO_6 is much more "rigid" than that of a conventional SG.[26]

There is relaxation of magnetization with applied magnetic field in the glassy state. Magnetization of a glassy state will respond to changes of applied field, roughly logarithmically in time. Moreover, the relaxation is strongly dependent on waiting time (t_w): the longer t_w, the slower is the relaxation (i.e., aging). Time-dependent relaxation measurements were performed according to ref 27. An external field of 10 Oe was applied after three different t_w (300, 1000, and 3000 s). Figure 3c,d illustrates strong t_w dependence below T_C. In Figure 3c, the rise of magnetization is slower with increasing t_w. In Figure 3d, time dependence of relaxation rate, $S(t) = \partial M/\partial \log t$, confirms that each inflection point approximately occurs at $t = t_w$, reflecting an intrinsic aging process similar to an SG state.[27]

Specific heat measurements also evidence a trace of magnetic dynamics, a smeared hump around T_C (Figure 3e). Generally, a "λ" shape peak is expected for a long-range magnetic ordering transition. The smeared hump may imply a transition from a paramagnetic to a "loose" long-range magnetic ordered state. At low temperature, the specific heat is only composed of lattice and magnetic parts (Figure S6a). The Debye temperature was calculated to be 381 K, a value close to that of A_2FeReO_6 (A = Ba, Ca) and $LaMn_{0.5}Co_{0.5}O_3$.[28,29] The absence of electronic contribution indicates insulating behavior for Y_2CoRuO_6, consistent with result of temperature-dependent resistivity measurements (Figure S6b).

$La_{2-x}Y_xCoRuO_6$ Solid Solutions. To trace back to the source of the magnetic dynamics in Y_2CoRuO_6, $La_{2-x}Y_xCoRuO_6$ (x = 0, 0.25, 0.5, 0.75, 1, 1.25, 1.5, and 1.75) series of samples were synthesized and investigated.

Crystal Structure. Laboratory PXD confirmed the monoclinic $P2_1/n$ symmetry of each $La_{2-x}Y_xCoRuO_6$ single phase. Lattice parameters of all the solid solutions were analyzed by Rietveld refinements (Figure S7). The details of the refinements are summarized in Supporting Information Table S5.

DOI: 10.1021/acs.chemmater.8b02728
Chem. Mater. 2018, 30, 7047−7054

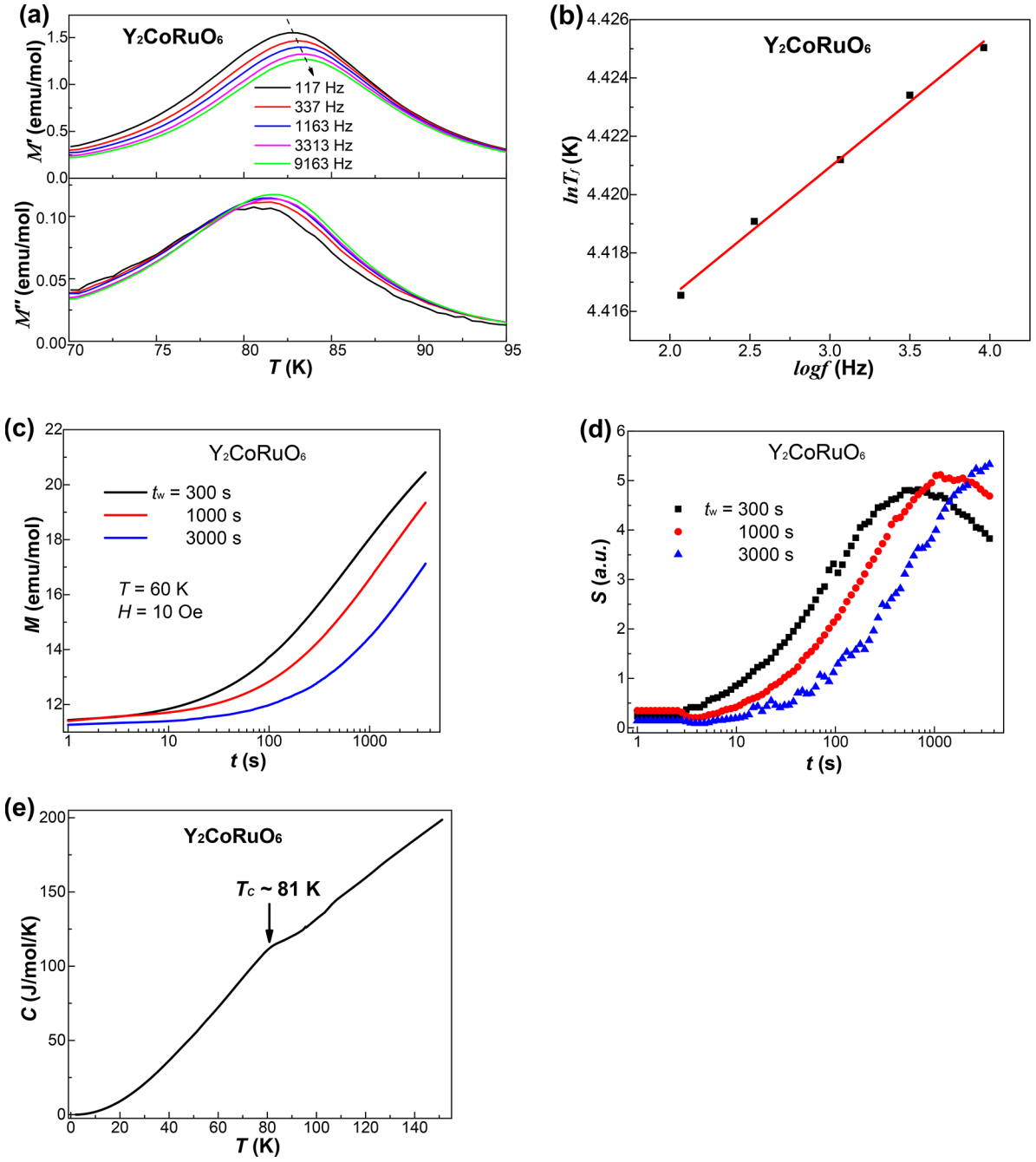

Figure 3. (a) Real and imaginary parts of AC susceptibility of Y_2CoRuO_6 measured with several frequencies. (b) Frequency dependence of transition temperature of Y_2CoRuO_6. (c) Isothermal magnetization of Y_2CoRuO_6 at T = 60 K and H = 10 Oe. (d) Corresponding relaxation rates $S(t)$. (e) Temperature dependence of specific heat of Y_2CoRuO_6 at H = 0 T. Black arrow corresponds to the transition temperature.

The average Co−O and Ru−O bond lengths are nearly independent of varying x, which suggests constant oxidation states of Co and Ru. The significant changes of lattice volume, and ϕ, the Co−O−Ru bond angles, are consistent with chemical compression by Y substitution as evidenced in Figure 4.

DC and AC Magnetism. Sample of x = 0. Consistent with a previous report,[22] La_2CoRuO_6 shows a sharp maximum (Neel temperature, T_N) at 25 K on $M(T)$ in Figure S8a,b. In Figure S8c, $M'(T)$ shows a consistent f-independent peak at 25 K. The $M''(T)$ in the entire measuring temperature range is noise-like, and its magnitude is close to zero. These behaviors indicate the presence of an AFM transition in La_2CoRuO_6.

Sample of x = 0.25, 0.5, and 0.75. These three samples have similar magnetic behavior in DC $M(T)$ and $M(H)$, and AC $M'(T)$ and $M''(T)$ (Figure S9a−d). $La_{1.75}Y_{0.25}CoRuO_6$ is discussed as a typical example: on lowering the temperature, DC $M(T)$ of H = 0.1 T shows divergence between ZFC and FC (T_{irr} ~ 72 K), one large bump (T_s ~ 45 K) on ZFC, and finally a small hump (~17 K) on ZFC and FC, respectively, in Figure 5a. T_{irr} and T_s rapidly shift toward lower temperature with larger H, reflecting SG-like behavior. In Figure 5b, $M'(T)$ and $M''(T)$ show one frequency-dependent peak at 17 K (first peak T_1, corresponding to the 17 K hump on DC $\chi(T)$) and another inconspicuous hump around 30 K (T_2) which is more notable on $M''(T)$. A broad hump around 17 K on $C/T(T)$

DOI: 10.1021/acs.chemmater.8b02728
Chem. Mater. 2018, 30, 7047−7054

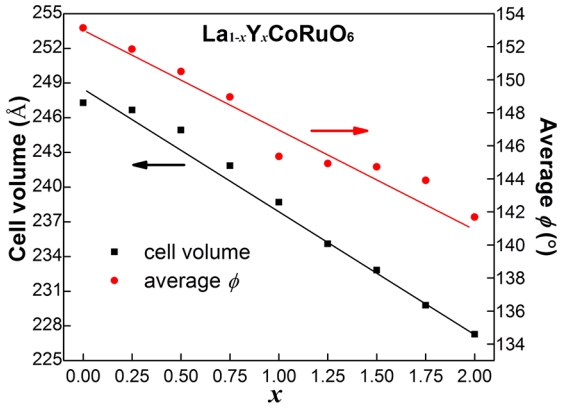

Figure 4. Cell volume and average Co−O−Ru bond angle, ϕ, as functions of yttrium concentration for $La_{2-x}Y_xCoRuO_6$.

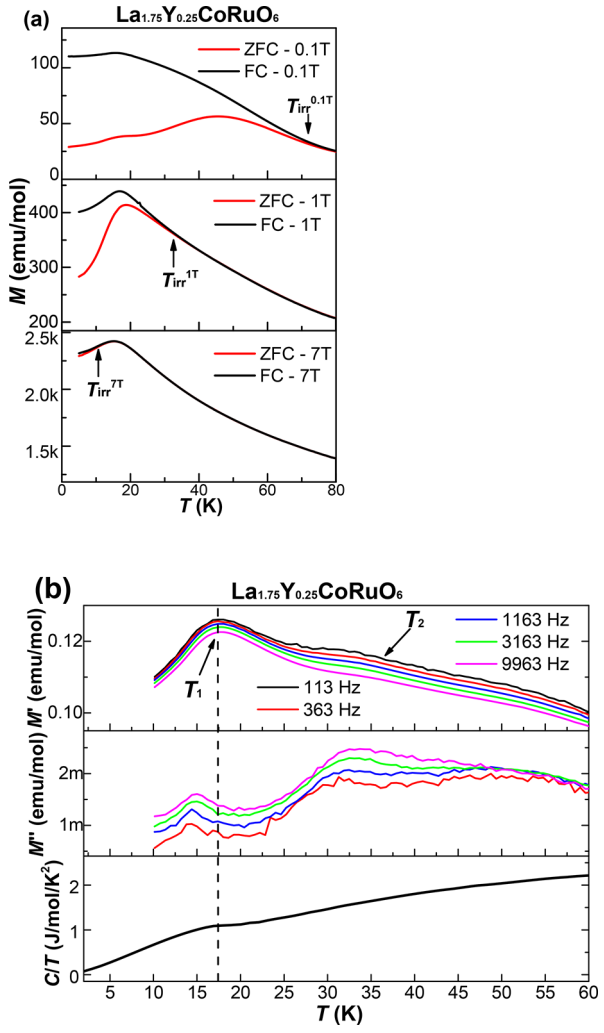

Figure 5. Physical properties of $La_{1.75}Y_{0.25}CoRuO_6$. (a) DC magnetization versus temperature with H = 0.1, 1, and 7 T. (b) Top two figures: AC magnetization versus temperature with varying applied frequencies. Bottom figure: specific heat of $La_{1.75}Y_{0.25}CoRuO_6$.

indicates that T_1 is a magnetic phase transition. In contrast, T_2 can only be referred to as a magnetic anomaly. Among the three samples, T_1 initially decreases with increasing x, and then increases a little for x = 0.75, while the loop in $M(H)$ enlarges with increasing x, which indicates a growing FM component (Figures S8 and S9). The frequency shift analysis with eq 2 is also performed for each f-dependent magnetic transition. For transitions which are indistinct on $M'(T)$, e.g., T_1 of $La_{1.25}Y_{0.75}CoRuO_6$, the corresponding peak shifts on $M''(T)$ are used for the fit.[31] Table S6 summarizes all the transition temperatures and corresponding characteristic parameters. When $x \leq 0.75$, K monotonically increases with increasing x.

Sample of x = 1, 1.25, 1.5, and 1.75. For each compound with $x \geq 1$, SG-like behavior, namely, H-dependent T_{irr} and T_s, still appear on DC $M(T)$ (Figure S10a−d). The loops in $M(H)$ steadily saturate with increasing x as shown in Figure S10e. $M'(T)$ of $La_{0.5}Y_{1.5}CoRuO_6$ is plotted in Figure S10f as a typical example. The AC susceptibility shows only a single cusp (T_1), which is also f-dependent and observed for each sample. The transition temperature increases with increasing x, while the magnitude of f dependence decreases with increasing x. All the K calculated with eq 2 are tabulated in Table S6. The decreasing K indicates that the SG-like phases become increasingly rigid and the magnetic moments in $La_{2-x}Y_xCoRuO_6$ gradually order.

The changes in dynamics of T_1 with varying x are also reflected in the evolutions of peaks on specific heat measurements. At the magnetic transition temperatures, a peak of the $C(T)$ of La_2CoRuO_6 degenerates into a broad hump on $La_{1.75}Y_{0.25}CoRuO_6$ and disappears with increasing Y substitution in Figure S11a. The trace of transition barely emerges again until x reaches 1.5 and gradually grows with increasing x (Figure S11b). The smeared or disappeared peaks on the $C(T)$ of $La_{2-x}Y_xCoRuO_6$ imply the presence of magnetic frustration.

DISCUSSION

It is interesting to note that the NPD results suggest a well-defined long-range FiM order in Y_2CoRuO_6 while the frequency dispersion, the aging phenomena, and the broad hump on $C(T)$ are convincing features of SG-like dynamics.[30] These SG-like behaviors are partly similar to scenarios in a few materials, whose long-range magnetic orders are labeled as "chaotic",[4,5,31−33] because frustration emerges below the transition of a long-range magnetic order. In the reported chaotic magnetic materials, the magnetic frustration is usually attributed to crystallographic disorder.[4,5] Particularly, the frustration in the FM analogue, La_2NiMnO_6, is believed to originate from partial disorder on the B-site.[34] In this work, it is argued that the mechanisms causing SG-like dynamics are the random antisite disorder of the two distinct magnetic ions and, more importantly, competition between the Co↑-O-(Ru)-O-Co↓/Ru↑-O-(Co)-O-Ru↓ superexchange interactions and the Co↑-O-Ru↓ one. The former is well-known to induce magnetic dynamics. We emphasize the contribution of the latter, because the strength of it shows correspondence with that of the magnetic dynamics in $La_{2-x}Y_xCoRuO_6$ solid solutions.

Figure 6 is the magnetic phase diagram of $La_{2-x}Y_xCoRuO_6$. At x = 0, La_2CoRuO_6 is an AFM semiconductor with T_N = 25 K. The Co/Ru spin structure was described by a ($^1/_2$, 0, $^1/_2$) propagation vector, but could not be solved unambiguously by the propagation vector (0, 0, 0).[22] On the left side of Figure 6, increasing K with increasing x indicates rising magnetic frustration, when the AFM order in La_2CoRuO_6 gradually degenerates into SG-like phases in the samples with x = 0.25, 0.5, and 0.75. On the right side, decreasing K with increasing x indicates decreasing magnetic frustration as the SG-like phase steadily changes into the FiM order in Y_2CoRuO_6. From

DOI: 10.1021/acs.chemmater.8b02728
Chem. Mater. 2018, 30, 7047−7054

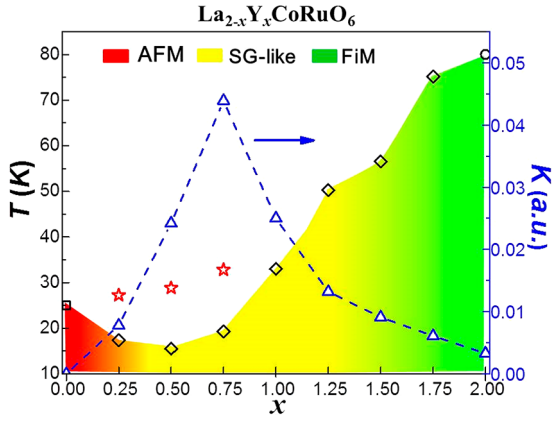

Figure 6. Magnetic phase diagram of $La_{2-x}Y_xCoRuO_6$. The black symbols are transition temperatures of $La_{2-x}Y_xCoRuO_6$ (square for T_N of $x = 0$, diamonds for T_1 of $0.25 \leq x \leq 1.75$, and circle for T_C of $x = 2$). Red stars are temperatures where magnetic anomalies occur. Red area is for AFM phase, yellow area for SG-like phase, green area for FiM phase, and white area for paramagnetic phase. The blue triangles represent the frequency shift, K, and the blue dashes reflect evolution of K of the corresponding transitions.

La_2CoRuO_6 to Y_2CoRuO_6, the process of AFM → SG-like → FiM reveals that the Co↑-O-(Ru)-O-Co↓/Ru↑-O-(Co)-O-Ru↓ AFM superexchange interactions are gradually overcome by the Co↑-O-Ru↓ one. The lattice compression bends the bond angles of Co−O−Ru and consequently favors the Co↑-O-Ru↓ pathway, similar to what is observed in $(Sr,Ca)_2CoOsO_6$ compounds.[14] The increasing Co↑-O-Ru↓ superexchange gradually defeats the AFM order in $La_{2-x}Y_xCoRuO_6$ and eventually forms FiM order in Y_2CoRuO_6. The competition between Co↑-O-Ru↓ superexchange and Co↑-O-(Ru)-O-Co↓/Ru↑-O-(Co)-O-Ru↓ interactions generates SG-like phases in $La_{2-x}Y_xCoRuO_6$, when the two types of superexchange interactions are comparable. Moving to the right side of Figure 6, the decreasing K values indicate diminished magnetic dynamics, which is not strong enough to disrupt the long-range ordered state in Y_2CoRuO_6, similar to that of the dynamic ferromagnet $Nd_{0.7}Sr_{0.3}MnO_3$.[33] Considering the frequency-independent nature of a canonical long-range magnetic order, the smaller K characterizes Y_2CoRuO_6 close to a static magnetic state. This conclusion is consistent with the NPD results.

CONCLUSIONS

In summary, the magnetic state of Y_2CoRuO_6 is intermediate between a canonical spin glass and long-range ferrimagnetic phase, but much closer to the latter. The combination of B-sites disorder with inherent magnetic competition generates the dynamic magnetic properties. Y_2CoRuO_6 presents a rarely observed route to reach magnetic dynamics rather than complete crystallographic disorder or geometrical frustration. The samples of $La_{2-x}Y_xCoRuO_6$ with $x = 0.25$, 1.5, and 1.75 are probably similar to Y_2CoRuO_6 with long-range magnetic orders and magnetic dynamics simultaneously. This of course requires further study from neutron diffraction. In addition, $La_{2-x}Y_xCoRuO_6$ presents a paradigm with abundant magnetic phases, and the entire solid solution offers an opportunity to tailor magnetic properties.

ASSOCIATED CONTENT

Supporting Information

The Supporting Information is available free of charge on the ACS Publications website at DOI: 10.1021/acs.chemmater.8b02728.

Chemical composition analysis by EDX; cation oxidation states analysis by XAS; neutron powder diffractions of Y_2CoRuO_6; temperature-dependent specific heat and resistivity of Y_2CoRuO_6; structural evolutions of $La_{2-x}Y_xCoRuO_6$ solid solutions; DC and AC magnetization of $La_{2-x}Y_xCoRuO_6$ solid solutions; specific heat of $La_{2-x}Y_xCoRuO_6$ solid solutions (PDF)

AUTHOR INFORMATION

Corresponding Author

*E-mail: greenbla@chem.rutgers.edu.

ORCID

Peter W. Stephens: 0000-0002-8311-7305
Man-Rong Li: 0000-0001-8424-9134
Martha Greenblatt: 0000-0002-1806-2766

Notes

The authors declare no competing financial interest.

ACKNOWLEDGMENTS

This work was supported by NSF-DMR-1507252 grant. The works at IOPCAS were supported by NSF & MOST of China through research projects. Portions of this research used U.S. Department of Energy Office of Science user facilities as follows: The Advanced Photon Source (Contract No. DE-AC02-06CH11357); NSLS-I (DE-AC02-98CH10886); NSLS-II (DE-SC0012704); High Flux Isotope Reactor, operated by the Oak Ridge National Laboratory. The authors wish to gratefully acknowledge J.-G. Cheng, Y. W. Long, and J. Friedland for helpful discussions.

REFERENCES

(1) Balents, L. Spin liquids in frustrated magnets. *Nature* **2010**, *464*, 199−208.

(2) Bramwell, S. T.; Gingras, M. J. P. Spin Ice State in Frustrated Magnetic Pyrochlore Materials. *Science* **2001**, *294*, 1495−1501.

(3) Mydosh, J. A. *Spin Glasses: An Experimental Introduction*; Taylor & Francis: London, 1993.

(4) Jonason, K.; Mattsson, J.; Nordblad, P. Chaos in the Ferromagnetic Phase of a Reentrant Ferromagnet. *Phys. Rev. Lett.* **1996**, *77*, 2562−2565.

(5) Upadhyay, S. K.; Iyer, K. K.; Rayaprol, S.; Paulose, P. L.; Sampathkumaran, E. V. A rock-salt-type Li-based oxide, $Li_3Ni_2RuO_6$, exhibiting a chaotic ferrimagnetism with cluster spin-glass dynamics and thermally frozen charge carriers. *Sci. Rep.* **2016**, *6*, 31883.

(6) Carlo, J. P.; Clancy, J. P.; Aharen, T.; Yamani, Z.; Ruff, J. P. C.; Wagman, J. J.; Van Gastel, G. J.; Noad, H. M. L.; Granroth, G. E.; Greedan, J. E.; Dabkowska, H. A.; Gaulin, B. D. Triplet and in-gap magnetic states in the ground state of the quantum frustrated fcc antiferromagnet Ba_2YMoO_6. *Phys. Rev. B: Condens. Matter Mater. Phys.* **2011**, *84*, 100404.

(7) Kermarrec, E.; Marjerrison, C. A.; Thompson, C. M.; Maharaj, D. D.; Levin, K.; Kroeker, S.; Granroth, G. E.; Flacau, R.; Yamani, Z.; Greedan, J. E.; Gaulin, B. D. Frustrated fcc antiferromagnet Ba_2YOsO_6: Structural characterization, magnetic properties, and neutron scattering studies. *Phys. Rev. B: Condens. Matter Mater. Phys.* **2015**, *91*, 075133.

(8) Aharen, T.; Greedan, J. E.; Bridges, C. A.; Aczel, A. A.; Rodriguez, J.; MacDougall, G.; Luke, G. M.; Michaelis, V. K.; Kroeker, S.; Wiebe, C. R.; Zhou, H.; Cranswick, L. M. D. Structure and

DOI: 10.1021/acs.chemmater.8b02728
Chem. Mater. 2018, 30, 7047−7054

magnetic properties of the S = 1 geometrically frustrated double perovskites La_2LiReO_6 and Ba_2YReO_6. *Phys. Rev. B: Condens. Matter Mater. Phys.* **2010**, *81*, 064436.
(9) Kato, H.; Okuda, T.; Okimoto, Y.; Tomioka, Y.; Oikawa, K.; Kamiyama, T.; Tokura, Y. Structural and electronic properties of the ordered double perovskites A_2MReO_6 (A = Sr,Ca; M = Mg,Sc,Cr,Mn,Fe,Co,Ni,Zn). *Phys. Rev. B: Condens. Matter Mater. Phys.* **2004**, *69*, 184412.
(10) Erickson, A. S.; Misra, S.; Miller, G.; Gupta, R. R.; Schlesinger, Z.; Harrison, W.; Kim, J. M.; Fisher, I. R. Ferromagnetism in the Mott Insulator Ba_2NaOsO_6. *Phys. Rev. Lett.* **2007**, *99*, 016404.
(11) Aharen, T.; Greedan, J. E.; Bridges, C. A.; Aczel, A. A.; Rodriguez, J.; MacDougall, G.; Luke, G. M.; Imai, T.; Michaelis, V. K.; Kroeker, S.; Zhou, H.; Wiebe, C. R.; Cranswick, L. M. D. Magnetic properties of the geometrically frustrated S = 1/2 antiferromagnets, La_2LiMoO_6 and Ba_2YMoO_6, with the B-site ordered double perovskite structure: Evidence for a collective spin-singlet ground state. *Phys. Rev. B: Condens. Matter Mater. Phys.* **2010**, *81*, 224409.
(12) Retuerto, M.; García-Hernández, M.; Martínez-Lope, M. J.; Fernández-Díaz, M. T.; Attfield, J. P.; Alonso, J. A. Switching from ferro- to antiferromagnetism in A_2CrSbO_6 (A = Ca, Sr) double perovskites: a neutron diffraction study. *J. Mater. Chem.* **2007**, *17*, 3555−3561.
(13) Morrow, R.; Freeland, J. W.; Woodward, P. M. Probing the links between structure and magnetism in $Sr_{2-x}Ca_xFeOsO_6$ double perovskites. *Inorg. Chem.* **2014**, *53*, 7983−7992.
(14) Morrow, R.; Yan, J.; McGuire, M. A.; Freeland, J. W.; Haskel, D.; Woodward, P. M. Effects of chemical pressure on the magnetic ground states of the osmate double perovskites $SrCaCoOsO_6$ and Ca_2CoOsO_6. *Phys. Rev. B: Condens. Matter Mater. Phys.* **2015**, *92*, 094435.
(15) Morrow, R.; Soliz, J. R.; Hauser, A. J.; Gallagher, J. C.; Susner, M. A.; Sumption, M. D.; Aczel, A. A.; Yan, J.; Yang, F.; Woodward, P. M. The effect of chemical pressure on the structure and properties of A_2CrOsO_6 (A = Sr, Ca) ferrimagnetic double perovskite. *J. Solid State Chem.* **2016**, *238*, 46−52.
(16) Feng, H. L.; Arai, M.; Matsushita, Y.; Tsujimoto, Y.; Guo, Y.; Sathish, C. I.; Wang, X.; Yuan, Y. H.; Tanaka, M.; Yamaura, K. High-temperature ferrimagnetism driven by lattice distortion in double perovskite Ca_2FeOsO_6. *J. Am. Chem. Soc.* **2014**, *136*, 3326−3329.
(17) Toby, B. EXPGUI, a graphical user interface for GSAS. *J. Appl. Crystallogr.* **2001**, *34*, 210−213.
(18) Rietveld, H. M. A profile refinement method for nuclear and magnetic structures. *J. Appl. Crystallogr.* **1969**, *2*, 65−71.
(19) Rodríguez-Carvajal, J. Recent advances in magnetic structure determination by neutron power diffraction. *Phys. B* **1993**, *192*, 55−69.
(20) Lufaso, M. W.; Barnes, P. W.; Woodward, P. M. Structure prediction of ordered and disordered multiple octahedral cation perovskites using SPuDS. *Acta Crystallogr., Sect. B: Struct. Sci.* **2006**, *62*, 397−410.
(21) Glazer, A. M. The classification of tilted octahedra in perovskites. *Acta Crystallogr., Sect. B: Struct. Crystallogr. Cryst. Chem.* **1972**, *28*, 3384−3392.
(22) Bos, J.-W. G.; Attfield, J. P. Crystal and magnetic structures of the double perovskite La_2CoRuO_6. *J. Mater. Chem.* **2005**, *15*, 715−720.
(23) Brese, N. E.; O'Keeffe, M. Bond-Valence Parameters for Solids. *Acta Crystallogr., Sect. B: Struct. Sci.* **1991**, *47*, 192−197.
(24) Neel, L. Antiferromagnetism and Ferrimagnetism. *Proc. Phys. Soc., London, Sect. A* **1952**, *65*, 869−885.
(25) Dass, R. I.; Yan, J. Q.; Goodenough, J. B. Ruthenium double perovskites: Transport and magnetic properties. *Phys. Rev. B: Condens. Matter Mater. Phys.* **2004**, *69*, 094416.
(26) Lekshmi, P. N.; Raji, G. R.; Vasundhara, M.; Varma, M. R.; Pillai, S. S.; Valant, M. Re-entrant spin glass behaviour and magneto-dielectric effect in insulating Sm_2NiMnO_6 double perovskite. *J. Mater. Chem. C* **2013**, *1*, 6565−6574.
(27) Krishna Murthy, J.; Venimadhav, A. Reentrant cluster glass behavior in La_2CoMnO_6 nanoparticles. *J. Appl. Phys.* **2013**, *113*, 163906.
(28) Prellier, W.; Smolyaninova, V.; Biswas, A.; Galley, C.; Greene, R. L.; Ramesha, K.; Gopalakrishnan, J. Properties of the ferrimagnetic double perovskites A_2FeReO_6 (A = Ba and Ca). *J. Phys.: Condens. Matter* **2000**, *12*, 965−973.
(29) Manna, K.; Elizabeth, S.; Anil Kumar, P. S. Anomalous re-entrant glassy magnetic phase in $LaMn_{0.5}Co_{0.5}O_3$ single crystals. *J. Appl. Phys.* **2016**, *119*, 043906.
(30) Mathieu, R.; Nordblad, P.; Nam, D. N. H.; Phuc, N. X.; Khiem, N. V. Short-range ferromagnetism and spin-glass state in $Y_{0.7}Ca_{0.3}MnO3$. *Phys. Rev. B: Condens. Matter Mater. Phys.* **2001**, *63*, 174405.
(31) Jonason, K.; Mattsson, J.; Nordblad, P. Dynamic susceptibility of a reentrant ferromagnet. *Phys. Rev. B: Condens. Matter Mater. Phys.* **1996**, *53*, 6507−6513.
(32) Kaul, S. N.; Semwal, A. Magnetic relaxation in a three-dimensional ferromagnet with weak quenched random-exchange disorder. *Pramana* **2003**, *61*, 1129−1144.
(33) Nam, D. N. H.; Mathieu, R.; Nordblad, P.; Khiem, N. V.; Phuc, N. X. Ferromagnetism and frustration in $Nd_{0.7}Sr_{0.3}MnO_3$. *Phys. Rev. B: Condens. Matter Mater. Phys.* **2000**, *62*, 1027−1032.
(34) Choudhury, D.; Mandal, P.; Mathieu, R.; Hazarika, A.; Rajan, S.; Sundaresan, A.; Waghmare, U. V.; Knut, R.; Karis, O.; Nordblad, P.; Sarma, D. D. Near-room-temperature colossal magnetodielectricity and multiglass properties in partially disordered La_2NiMnO_6. *Phys. Rev. Lett.* **2012**, *108*, 127201.

DOI: 10.1021/acs.chemmater.8b02728
Chem. Mater. 2018, 30, 7047−7054